AFRL-AFOSR-VA-TR-2023-0230

An experimental/computational investigation of the response of a compliant panel to turbulent and transitional shock-wave/boundary-layer interactions in hypersonic flow

STUART LAURENCE
UNIVERSITY OF MARYLAND, COLLEGE PARK
3112 LEE BLDG 7809 REGENTS DR
COLLEGE PARK, MD, 20742
USA

12/16/2022
Final Technical Report

Air Force Research Laboratory
Air Force Office of Scientific Research
Arlington, Virginia 22203
Air Force Materiel Command

REPORT DOCUMENTATION PAGE

PLEASE DO NOT RETURN YOUR FORM TO THE ABOVE ORGANIZATION.

1. REPORT DATE	**2. REPORT TYPE**	**3. DATES COVERED**	
20221216	Final	**START DATE** 20210519	**END DATE** 20220518

4. TITLE AND SUBTITLE
An experimental/computational investigation of the response of a compliant panel to turbulent and transitional shock-wave/boundary-layer interactions in hypersonic flow

5a. CONTRACT NUMBER	**5b. GRANT NUMBER**	**5c. PROGRAM ELEMENT NUMBER**
	FA9550-21-1-0249	61102F
5d. PROJECT NUMBER	**5e. TASK NUMBER**	**5f. WORK UNIT NUMBER**

6. AUTHOR(S)
Stuart Laurence, Daniel Bodony

7. PERFORMING ORGANIZATION NAME(S) AND ADDRESS(ES)	**8. PERFORMING ORGANIZATION REPORT NUMBER**
UNIVERSITY OF MARYLAND, COLLEGE PARK 3112 LEE BLDG 7809 REGENTS DR COLLEGE PARK, MD 20742 USA	

9. SPONSORING/MONITORING AGENCY NAME(S) AND ADDRESS(ES)	**10. SPONSOR/MONITOR'S ACRONYM(S)**	**11. SPONSOR/MONITOR'S REPORT NUMBER(S)**
Air Force Office of Scientific Research 875 N. Randolph St. Room 3112 Arlington, VA 22203	AFRL/AFOSR RTA1	AFRL-AFOSR-VA-TR-2023-0230

12. DISTRIBUTION/AVAILABILITY STATEMENT
A Distribution Unlimited: PB Public Release

13. SUPPLEMENTARY NOTES

14. ABSTRACT
Experiments at Mach 6 and 10 on a flat-plate/ramp configuration with an embedded compliant panel are conducted to investigate the fluid-thermal-structural interaction (FTSI) induced by a nominally two-dimensional shockwave/ boundary-layer interaction (SWBLI) for various ramp angles and panel back pressures. Stereo photogrammetry, focusing schlieren, surface pressure measurements, and IR thermography are used to characterize the panel mechanical and thermal state as well as the unsteady flowfield characteristics. Corresponding simulations of the Mach 6 flow approaching and interacting with a 35 degree ramp to develop a fundamental understanding of the fluid-ramp interaction. Finally, an unsteady aerodynamic model is developed that improves the quantitative accuracy of fluid-thermal-structural interaction predictions at conditions for which piston theory is known to be in error.

15. SUBJECT TERMS

16. SECURITY CLASSIFICATION OF:			**17. LIMITATION OF ABSTRACT**	**18. NUMBER OF PAGES**
a. REPORT U	**b. ABSTRACT** U	**c. THIS PAGE** U	UU	9

19a. NAME OF RESPONSIBLE PERSON	**19b. PHONE NUMBER** *(Include area code)*
SARAH POPKIN	000-0000

DISTRIBUTION A: Distribution approved for public release.

Technical Report: An experimental/computational investigation of the response of a compliant panel to turbulent and transitional shock-wave/boundary-layer interactions in hypersonic flow

Accomplishments

Research Objectives

The primary research objectives of this effort are as follows:

1. Conduct experiments at Mach 6 and 10 on a flat-plate/ramp configuration with an embedded compliant panel to investigate the fluid-thermal-structural interaction (FTSI) induced by a nominally two-dimensional shock-wave/boundary-layer interaction (SWBLI) for various ramp angles and panel back pressures.
2. Simulate the Mach 6 flow approaching and interacting with a 35 degree ramp to develop a fundamental understanding of the fluid-ramp interaction
3. Develop an unsteady aerodynamic model that improved the quantitative accuracy of fluid-thermal-structural interaction predictions at conditions for which piston theory was known to be in error.

Specific Accomplishments

Experiments

Two experimental campaigns were completed at the NASA Langley Research Center during this period of performance: the first in the Mach10 31-Inch Hypersonic Tunnel (March 7-8, 2022) and the second in the Mach 6 20-Inch Hypersonic Tunnel (April 11-15, 2022). In both campaigns, the model geometry was a flat plate at zero incidence fitted with a two-dimensional compression ramp of adjustable angle. The configuration for the Mach 6 experiments in shown in figure 1; in the Mach 10 configuration, the ramp was shifted downstream to allow larger Reynolds numbers to be obtained at the interaction location. The 15-5 PH/H1025 (AMS 5659) stainless-steel ramp had a cavity machined out of the rear surface to create a 0.5-mm thick compliant panel of dimensions 76.2 mm × 83.9 mm on the upper surface; in all cases, the upstream edge of the panel lay at the intersection of the flat plate and ramp. The cavity was sealed and fitted with a pressure-regulation device to allow the panel back pressure to be set to a specified value. The cavity pressure was monitored during a given experiment by means of two Kulite® XCE pressure transducers. The surface of the flat plate upstream of the ramp was instrumented with a streamwise row (along the centerline) of Kulite® and fast-response PCB 132B38 pressure transducers; two additional Kulites® were mounted on the ramp downstream of the panel (one on the centerline, the other at the panel quarter span).

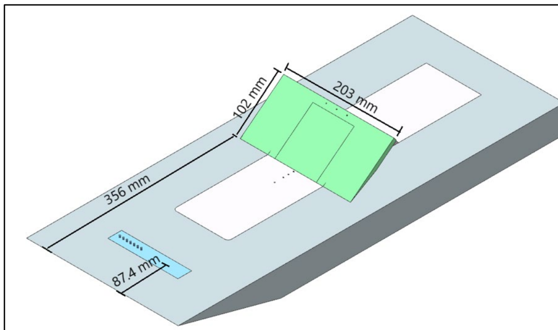

Figure 1: Model setup for the Mach 6 experiments.

In both campaigns, a high-speed focusing schlieren system (Bathel & Weisberger, 2021) was used to visualize the flow structures that developed in the corner region, and a high-speed stereoscopic photogrammetry setup was employed to record the global out-of-plane motion of the panel (Whalen et al., 2020). For the latter, a regular grid of circular markers was painted on the panel surface, and two Phantom high-speed cameras were used to record images with illumination provided by a high-intensity LED light source. The setup for the Mach 6 tunnel is shown in figure 2. For only the Mach 6 experiments, an IR camera (FLIR A655sc) was used to provide simultaneous measurements of the ramp surface temperature (an appropriate IR-transparent window wasn't available for the Mach 10 facility); to increase the IR signal, the ramp was painted with a thin layer of Rust-Oleum™ High Heat black paint, resistant to temperatures up to 1200 deg. F. IR images were recorded at 50 Hz, insufficient to resolve transient heating features (e.g., from the motion of the separation bubble) but adequate to determine the thermal state of the panel.

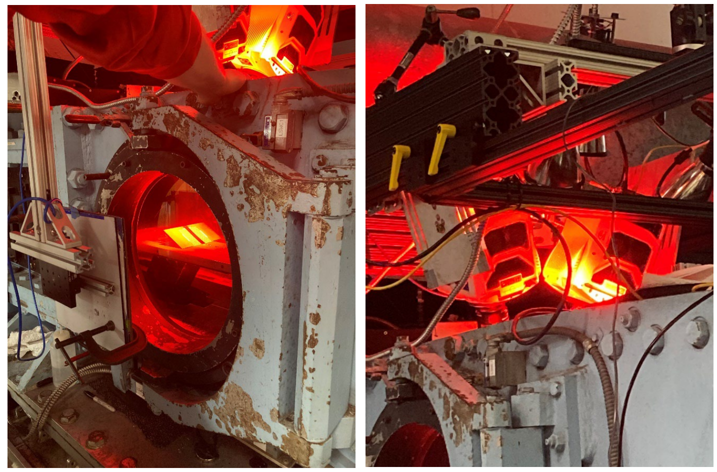

Figure 2: (Left) Test section of the Mach 6 20-Inch Hypersonic Tunnel with model and diagnostic equipment installed; (right) close-up of cameras mounted above the test section.

We first discuss the Mach 10 experiments. A total of 12 tests were performed, all at a unit Reynolds number of 5.0×10^5 m^{-1}. A set of "pizza-box" trips, spanning the width of the panel downstream of the leading edge, was included to induce a turbulent boundary-layer state. Three ramp angles (θ = 10°, 20°, and 30°) were tested; for each, four values for the panel back pressure, p_b, were specified, in each case equal to (approximately) 0, $p_2/3$, 2 $p_2/3$, and p_2, where p_2 is the inviscid pressure behind the oblique shock generated by the ramp (i.e., for an inviscid flow, $p_b=p_2$ means there would be no pressure differential across the panel). We are still waiting for NASA to release the photogrammetry and schlieren images from these experiments, so here we will provide only a preliminary discussion based on the available pressure-transducer data. In the left part of figure 3, we see the power spectral density spectra as measured by the transducers inside the plenum box for θ = 10° and zero nominal pressure difference across the compliant panel ($p_b=p_2$). In the XCE-85 signal, we see evidence of spectral content near 600 Hz and 1300 Hz, which would be consistent with oscillations of the (1,1) and (1,2) panel modes producing pressure fluctuations inside the cavity. In the right part of figure 3, we present the spectra recorded by the surface transducers mounted downstream of the panel for this same experiment. No clear signature of either of the modes seen in the plenum box are observed here, though we note that the centerline transducer exhibited anomalously high signal levels in the run. The behavior exhibited in figure 3 was generally typical of the other conditions tested, with at least one prominent peak in the plenum box spectra but no distinct peaks in the downstream spectra. Analysis of the photogrammetry and schlieren data, once available, will give much more detailed insight into the panel excitation and any signature in the flowfield over the ramp.

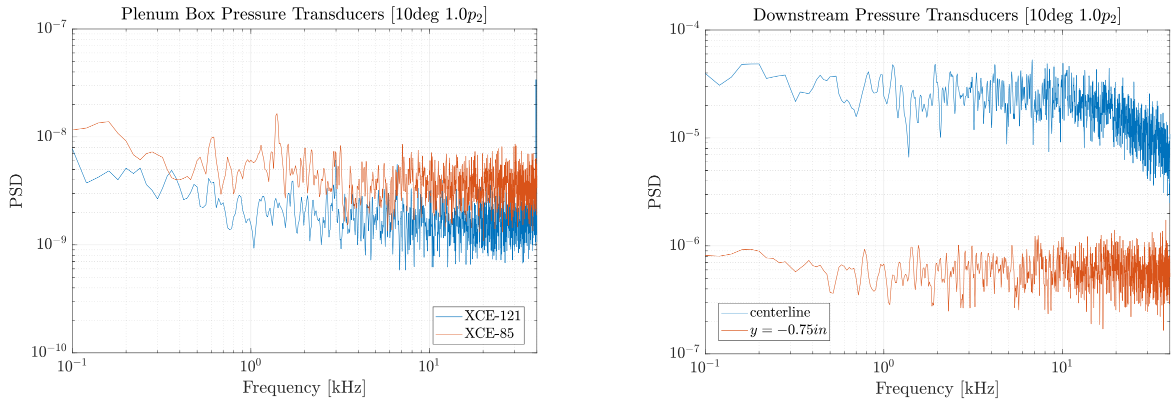

Figure 3: (Left) Frequency spectra measured in the plenum box behind the compliant panel at Mach 10 for θ = 10° and p_b=p_2; (right) spectra measured by surface transducers downstream of the panel at the same condition.

The Mach 6 campaign was larger in scope, allowed the examination of an additional parameter besides the ramp angle and panel back pressure, namely the incoming boundary layer state. This was varied by testing at two different unit Reynolds numbers, 6.6×10^6 m^{-1} and 23.8×10^6 m^{-1}; the smaller of these resulted in a transitional incoming boundary layer, while the larger provided a fully turbulent boundary layer. Additional experiments were performed at the lower Reynolds number with trips on half the span of the flat plate to generate a laterally nonuniform boundary-layer state on the panel, i.e., partially transitional and partially turbulent. As for the Mach 10 tests, we are still waiting for the schlieren and photogrammetry image data to be cleared for release by NASA, but we have performed a preliminary analysis on the pressure and IR data.

Figure 4 shows PSD spectra measured by Kulite® transducers inside the plenum box and downstream of the panel for θ = 20° at the higher unit Reynolds number, with a pressure differential across the panel of 7.4 kPa and no trips. Again, we see a strong peak in one of the plenum transducers (XCE-621) at a frequency (~600 Hz) corresponding to the (1,1) panel mode (the XCE-618 transducer is defective here); however, we now note an associated peak in the centerline transducer downstream of the panel, indicating that now the panel oscillations are sufficiently large to impart a significant footprint in the downstream flow. Removing the nominal pressure differential reduced the strength of this downstream peak, but it was still clearly present in the centerline Kulite spectrum.

In figure 5, we show sample IR thermography results from the same experiment. In the left plot, the temperature rise along the panel (averaged over the span) is presented at several experimental times. As we would expect, a monotonic increase in temperature with time is observed, though the difference between consecutive timesteps becomes small at later times, indicating that parts of the panel are approaching the adiabatic recovery temperature. At each time step, we see a steady rise in temperature along the panel for most of its length. In the right plot, the mean difference in temperature between the panel and its surrounding structure is shown (note that, because the panel is thinner than its housing, it heats up more rapidly). This latter temperature difference is important for determining whether the panel is at risk of undergoing thermal buckling; simulations by Earl Dowell's group have indicated a buckling limit of less than 30 K for these conditions.

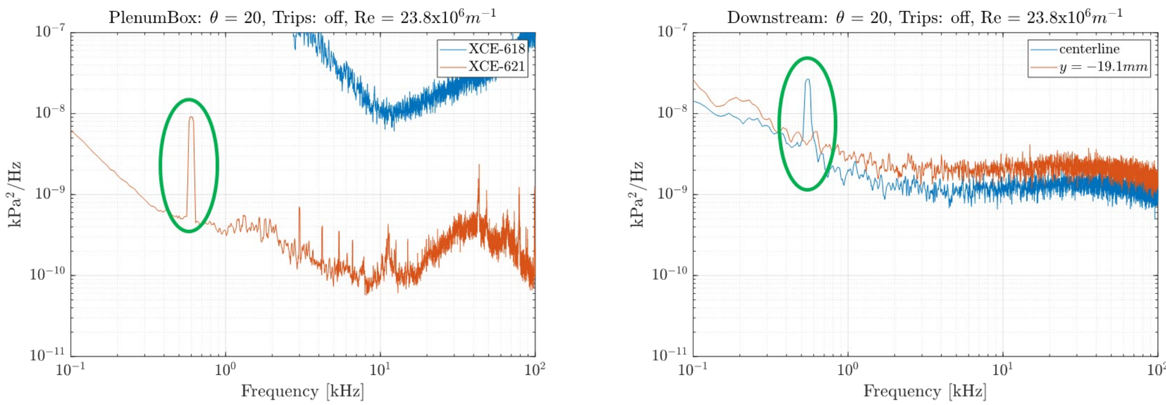

Figure 4: (Left) Frequency spectra measured inside the plenum box behind the compliant panel at Mach 6 for $\theta = 10°$, $Re/m = 23.8\times10^6$ m^{-1}, and $\Delta p = 7.4$ kPa; (right) surface pressure spectra immediately downstream of the panel at the same conditions.

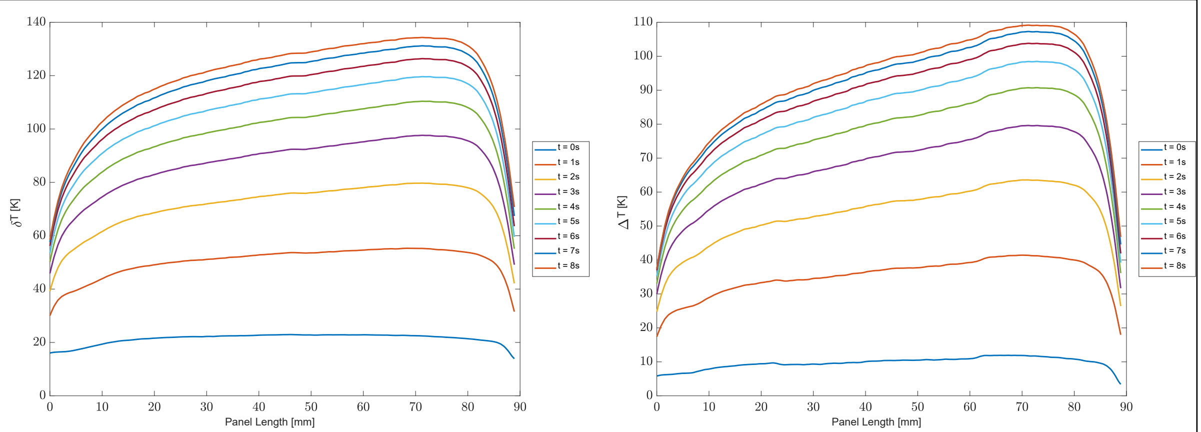

Figure 5: Measured temperatures along the panel (averaged over the span) at different experimental times: (left) change from initial temperature ($\delta T = T - T_{initial}$); (right) temperature difference between panel and adjacent structure

With such thermal buckling in mind, we can also apply a short-time Fourier transform to the plenum pressure data to determine whether there is any obvious change in the panel frequencies as the panel heats up. Figure 6 shows the short-time PSD derived in this fashion for the experiment described above, plotted here against the difference in mean temperature between the panel and housing. No obvious changes are observed in this case, but the plenum pressure is a rather indirect way of determining such frequencies. We will repeat this process with the frequencies derived from the photogrammetry data when they become available in the hope of resolving any obvious buckling-related events during experiments.

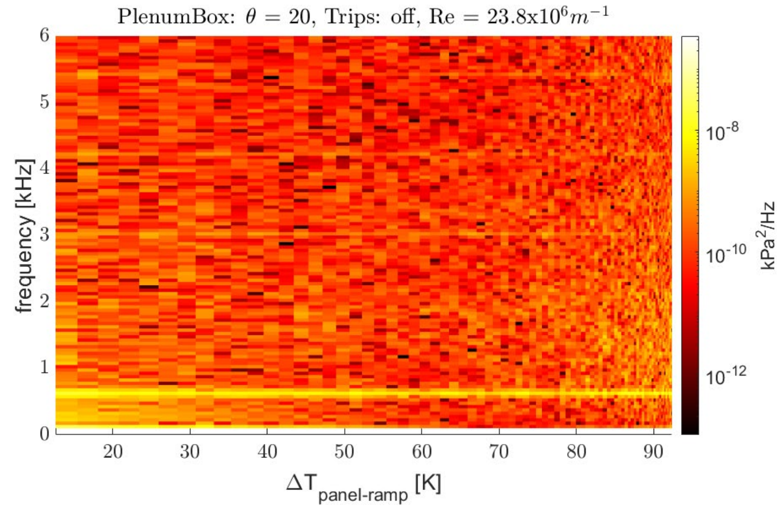

Figure 6: Short-time PSD of the plenum-pressure signal versus the difference in temperature between the panel and housing during the same experiment as in figures 4 and 5.

Simulations

Simulations of the Mach 6 flow approaching the 35 degree ramp were conducted using PI Bodony's compressible DNS solver. The solver utilizes a bandwidth-optimized WENO formulation, with corrections for stability and enhancements for turbulence-resolving capabilities (Murthy and Bodony, 2022; described below), expressed in generalized curvilinear coordinates on overset structured meshes (Bodony et al., 2011). The boundary conditions utilize a ghost cell technique appropriate for FTSI simulations (Vollmer et al., 2022). The code is written in C++ and Fortran 90 and utilizes MPI (Gropp et al., 1999), OpenMP (Dagum et al., 1999), and HDF5 (The HDF Group, 1997) for parallel communication, computation, and input/output, respectively.

Our unsteady aerodynamic modeling approach originates with the Euler equations linearized about a uniform velocity field with isentropic fluctuations. It can be shown that under these approximations, the deviation of the pressure $p'(x,t)$ from a uniform mean $\overline{\mathrm{p}}$ is given by the convective wave equation

$$\left(\frac{1}{\bar{c}^2}\frac{D^2p'}{Dt^2} - \frac{\partial^2}{\partial x_j\,\partial x_j}\right)p' = 0$$

with uniform sound speed $\bar{c}$. Here, $Dp'/Dt = \partial p'/\,\partial t + U\,\partial p'/\,\partial x_1$ is the convective derivative for a flow moving in the x_1 direction. Boundary conditions at the fluid-solid surface connect the normal pressure gradient $\partial p'/\,\partial n$ to the shape and motion of the surface $y = \eta(x,z,t)$ where, for simplicity, we assume the undeformed interface lies at $y = 0$.

Dowell (1974) showed that when using integral transform techniques in the x, z, and t directions, the lowest-order term of the solution yields piston theory result that $p'_{PT} \approx \overline{\rho}UD\eta/Dt$. Our objective is to use simulation data to develop a model for the error between p'_{PT} and the actual data $p'(x,0,z,t)$.

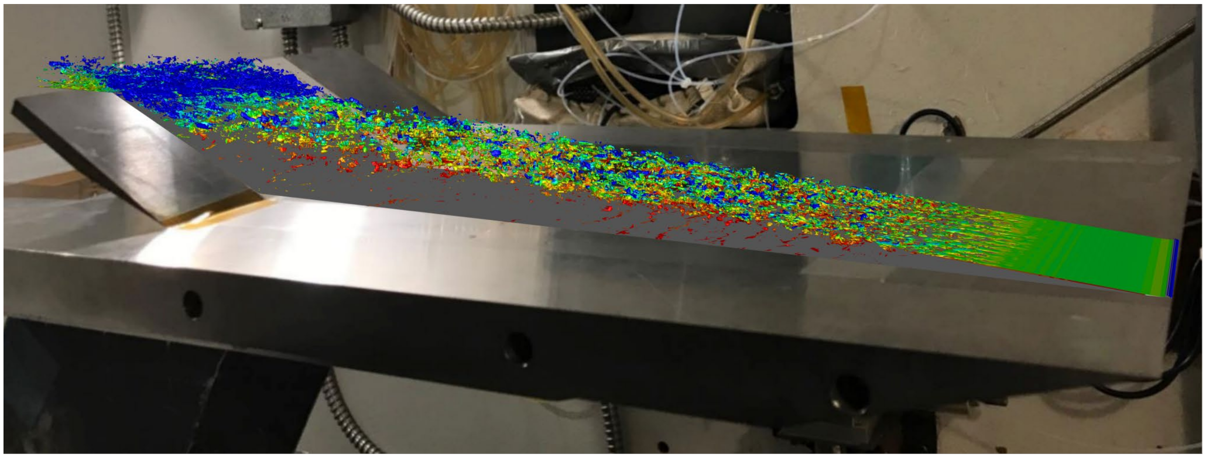

Figure 7: Visualization of the DNS-simulated Mach 6 flow at 20 million unit Reynolds number approaching the 35 degree ramp mounted to a flat plate with sharp leading edge.

Figure 7 shows the details of the flow under consideration for the first computational research objective. The flow domain includes the plate onto which the ramp is fixed, including the plate's leading edge, to capture the boundary layer development, shock-on-ramp impingement, and upstream separation. At Mach 6 and a unit Reynolds number of 20 million per meter, the plate-generated boundary layer is known to be turbulent at the forward ramp corner (Whalen et al., 2020); however, Figure 7 shows that the simulated boundary layer has fully separated with a turbulent separation bubble that extends upstream towards the plate leading edge and downstream, encompassing approximately 50% of the panel. This disagreement between the simulation and the experiment was traced to the free stream tunnel environment (Rufer and Berridge, 2012).

In the simulations, the original freestream was "quiet", i.e., absent of any disturbances generated by the tunnel sidewalls or other surfaces. Measurements within the NASA LaRC Mach 6 20-Inch Hypersonic Tunnel indicated, however, that there existed an extensive disturbance pressure field as measured by rake-mounted pitot probes and plate-mounted PCB pressure sensors (Rufer and Berridge, 2012). Using the pressure spectra as a guide, and assuming that the freestream pressure field was comprised of planar acoustic waves generated from each of the four sidewalls, a model pressure field was generated and applied into the simulations, upstream of the flat plate leading edge. Evolution of the simulation showed that the near-leading edge boundary layer separation point began moving downstream, albeit slowly, as the pressure field scattered into all three disturbance modes and interacted with the leading-edge boundary layer to initiate an upstream transition location, relative to the quiet state.

While waiting for the transition location to stabilize, the simulation showed signs of numerical instability and was paused. A deep-dive into the cause led us to discover that the original bandwidth-optimized WENO scheme we were using (Martìn et al., 2006) was numerically unstable over a small range of wavenumbers, with a growth rate so slow that only the very long simulations required for FTSI studies exposed the instability. After verifying the origin of the instability within the WENO coefficients, we generated a fully stable WENO bandwidth-optimized formulation and added a shock sensor to better localize the WENO around discontinuities and remove its negative impact on low-speed turbulence. At the time of this report, the restarted DNS was running.

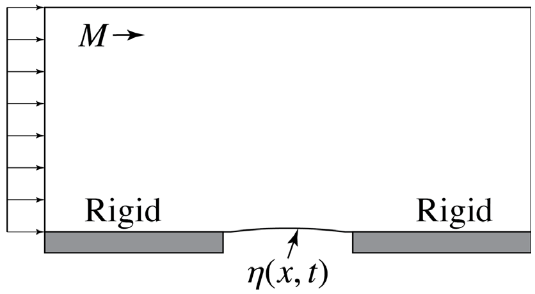

Figure 8: Configuration for CFD simulations used to generate a data-learned error model to improve upon piston theory.

For the unsteady aerodynamic modeling task, the general solution to the convective wave equation, for the scenario described above, can be written in the representation form as

$$p'(x,y,z,t) = \int_S G_S(\tilde{\vec{x}},\tilde{t}|\vec{x},t)\mathrm{L}(\eta(\tilde{x},\tilde{z},\tilde{t}))d\tilde{S} + \int_V G_V(\tilde{\vec{x}},\tilde{\tau}|\vec{x},t)p'd\tilde{V}.$$

Here, the Gs are surface and volume Green's functions, L is a differential operator, and as $\tilde{\vec{x}}$ approaches the surface $y = 0$, one finds an integral equation for $p'(x,0,z,t)$. Though a solution exists in principal, a simple closed form expression valid over all Mach numbers is not available. Instead, we use DMD (Schmid, 2010) to construct an error model of $p'(x,0,z,t) - p'_{PT}(x,z,t)$ using CFD-based data for simulations for the form shown in Figure 8. If we define $\overrightarrow{e_k} = p'(x,0,z,t_k) - p'_{PT}(x,z,t_k)$ as the surface pressure error between the actual and that predicted by piston theory, then we can assume that there exists a linear operator A that best approximates

$$\vec{e}_{k+1} = A\overrightarrow{\mathrm{e}_\mathrm{k}}$$

and use the DMD algorithm to find A. We chose the $\eta(x,t)$ to correspond to the fundamental *in vacuo* bending modes of a clamped beam, run the simulations, and collect the data vectors $\overrightarrow{e_k}$. Once the DMD-estimated A is known, then we can approximate the surface pressure as

$$p'(x,0,z,t_{k+1}) = A\overrightarrow{e_k} + p'_{PT}(x,z,t_{k+1})$$

where the form makes clear that the error term includes the memory effects of integrals of G_S and G_V given above as well as the neglect of the panel acceleration term that is buried within the operator L.

Figure 9 shows an example of the information learned from the DMD representation of the error, as well as the improvement in the surface pressure prediction when the error model is included. A dual-mode panel deflection case at Mach 1.3 is shown with clear evidence of the improvement. Further analysis (not shown) indicates that the most important DMD modes have shapes that remain robust with Mach number and we are currently seeking a method to predict those modes analytically so that the data learning process is not necessary for the example in Figure 8 and evaluated in Figure 9.

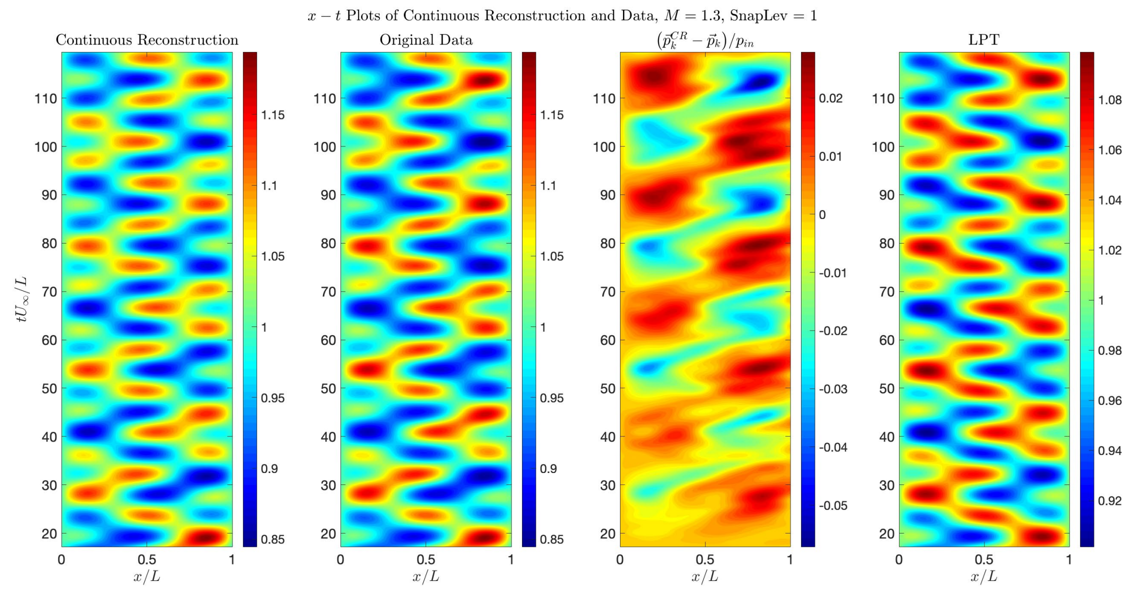

Figure 9: Demonstration of DMD-learned surface pressure error improving panel pressure predictive accuracy. A dual mode panel flutter case at Mach 1.3 is shown, with (from L to R): the DMD-enhanced prediction in the far-left pane, the original CFD surface pressure data, their difference, and the piston theory prediction. Observe that the amplitude and phase of the piston theory data are incorrect.

Dissemination of Research

Journal papers:

- Dettenrieder, F. and Bodony, D. J. (2022) "Stability analysis of compressible flat plate boundary layer flow over a mechanically compliant wall," invited paper for hypersonics-focused special issue of *Theoretical and Computational Fluid Dynamics.* https://doi.org/10.1007/s00162-021-00600-z

Conference papers:

- Vollmer, B., Murthy, S., and Bodony, D. J. "Revisiting the Boundary Conditions for Unsteady Flows Adjacent to Rigid and Dynamic Solid Walls," AIAA Paper 2022-2895, Presented at the 28th AIAA/CEAS Aeroacoustics Conference, June, 2022, Southampton, UK.

Presentations:

- Invited Presentation, "Direct Numerical Simulation of Hypersonic Flows Using Frontera," presented at the National Science Foundation Frontera User Meeting, University of Texas at Austin, August 4-5, 2022.

- Invited Presentation, “Numerical Simulations of Turbulent, Multiphysics Hypersonic Flows at Extreme Scales,” presented at the DFD/DCOMP focus session on “Extreme-Scale Computational Science Discovery in Fluid Dynamics and Related Disciplines,” at the APS March Meeting, Chicago, IL, March 14-18, 2022.

Impacts

The experiments described here constitute a unique and extensive data set for high-speed fluid-thermal-structure interactions. Analysis of the fluid and structural behavior at these conditions will provide critical data for informing reduced-order models of FTSI and give important validation data for high-fidelity numerical simulations. The data-enriched piston theory proposed here, meanwhile, has the potential to significantly enhance our ability to accurately and efficiently model hypersonic fluid-structure-interaction problems.

References Cited

B. Bathel and J. Weisberger, “Compact, self-aligned focusing schlieren system,” Optics Letters, Vol. 46, No. 14, pp. 3328--3331, 2021

S. J. Rufer and D. C. Berridge, “Pressure Fluctuation Measurements in the NASA Langley 20-Inch Mach 6 Wind Tunnel,” AIAA Paper 2012-3262, Presented at the 42nd AIAA Fluid Dynamics Conference and Exhibit, 25--28 June 2012, New Orleans, LA.

M. P. Martìn and E. M. Taylor and M. Wu and V. G. Weirs, “A bandwidth-optimized WENO scheme for the effective direct numerical simulation of compressible turbulence,” Journal of Computational Physics, Vol. 220, pp. 270—289, 2006.

E. H. Dowell, *Aeroelasticity of Plates and Shells*, Noordhoff International Publishing, 1974.

P. J. Schmid, “Dynamic mode decomposition of numerical and experimental data,” Journal of Fluid Mechanics, Vol. 656, pp. 5—28, 2010.

The HDF Group. Hierarchical Data Format, version 5, 1997-NNNN, https://www.hdfgroup.org/HDF5/.

Leonardo Dagum and Ramesh Menon, “OpenMP: an industry standard API for shared-memory programming,” *Computational Science & Engineering, IEEE*, Vol. 5(1), pp. 46—55, 1999.

W. Gropp, E. Lusk, and R. Thakur, *Using MPI-2: Advanced Features of the Message-Passing Interface*, MIT Press, 1999.

T. J. Whalen, A. G. Schoeneich, S. J. Laurence, B. Sullivan, D. Bodony, M. Freydin, E. Dowell, and G. Buck, "Hypersonic Fluid-Structure Interactions in Compression Corner Shock-Wave/Boundary-Layer Interaction", AIAA Journal, 58(9):4090-4105, 2020.